

Structural and Magnetic Study of Manganese Substituted Zinc Ferrite ($Mn_xZn_{1-x}Fe_2O_4$)
Nanostructures Synthesized via Citric Acid assisted Solgel Autocombustion Method

Turkish Online Journal of Qualitative Inquiry (TOJQI)
Volume 12, Issue 10, October 2021: 5614-5632

**Structural and Magnetic Study of Manganese Substituted Zinc Ferrite
($Mn_xZn_{1-x}Fe_2O_4$) Nanostructures Synthesized via Citric Acid assisted Solgel
Autocombustion Method**

Tasaduk Ahmad Wani¹ and Dr. G. Suresh²

¹Ph.D. Research Scholar, Department of Physics, Annamalai University Annamalai Nagar (608002), Tamil Nadu
(India)

²Associate Professor, Department of Physics, Annamalai University, Annamalainagar (608002), Tamil Nadu
(India)

Abstract: A series of spinel nanocrystalline $Mn_xZn_{1-x}Fe_2O_4$ ($X = 0.00, 0.15, 0.30, 0.45$) mixed ferrites were successfully synthesized above 1000 °C by Solgel Autocombustion Synthesis route. The comprehensive characterizations of the ferrite nanostructures and study of the magnetic properties were carried out by XRD, SEM, and VSM like instrumentation techniques, respectively. The consequence of Mn^{2+} ion concentration on structural, morphological, and magnetic characterizations of Zn-Mn ferrite nanostructures was examined. XRD confirmed the single-phase spinel cubic structure of the samples with a particle size range of 28 to 35 nm. SEM micrographs confirmed nearly compact spherical-shaped nanoparticles. Magnetic measurement derived from Hysteresis-Loop revealed that there is an increase in saturation magnetization (M_s) with increasing Mn^{2+} concentration. The M-H loops for all the samples are narrow with low values of coercivity and retentivity, indicating the superparamagnetic nature of these samples. Thus, optimized substituting manganese for zinc in Mn-Zn nano-ferrites improves its magnetic properties and makes these nanoparticles a potential candidate for their applications in hyperthermia, drug delivery, and MRI.

Keywords: Soft Ferrites, Mn-Zn Ferrite, X-ray Diffraction, Magnetic Properties, Superparamagnetism

1.1. Introduction

Ferrites are the subject of much investigation due to their exciting and promising features. These nano-magnetic materials have attracted the interest of young magnetic material researchers due to their smart magnetic capabilities. Ferrites [1,2] are non-conducting ceramic ferrimagnetic materials composed primarily of iron oxide (Fe_2O_4), with minor amounts of metals such as cobalt (Co), manganese (Mn), nickel (Ni), zinc (Zn), and others. They have asymmetrical opposing magnetic moments, allowing spontaneous magnetization and hysteresis in such materials. Ferrites are divided into hard ferrites [3] and soft ferrites [4, 5]. Hard ferrites have a high coercivity and are challenging to magnetize after being demagnetized. As a result, these materials are excellent for fabricating permanent magnets, which are utilized in refrigerators, loudspeakers, washing machines, televisions, communication systems, switch-mode power supply, microwave absorption systems, high-frequency applications, and so on [6,7]. Hard ferrites are commonly found in the form of cobalt ferrites and barium ferrites.

On the other hand, soft ferrites are easy to magnetize or demagnetize due to their low coercive field strengths. They have a wide variety of applications in the electronic sector, including the development of transformer cores, high-frequency inductors, and microwave components [8, 9]. Soft ferrites also have excellent resistivity, cheap cost, temporal and temperature stability, low loss, and high permeability [10]. Mn-Zn ferrites [11] and Ni-Zn ferrites [12, 13, 14] have received the most attention among soft ferrites due to their high electrical resistivity (10^7 ohm), low-cost synthesis, minimal dielectric loss, exceptionally high mechanical strength, and chemical stability [15, 16].

Mn-Zn ferrites with the formula $\text{Mn}_x\text{Zn}_{1-x}\text{Fe}_2\text{O}_4$ have gained much attention in academia over the last decade due to their high initial permeability and low hysteresis losses, which make Mn-Zn ferrites appropriate for use in many everyday applications. Manganese-zinc ferrites have more excellent permeability and saturation induction than Ni-Zn ferrites [17]. Mn-Zn ferrites are employed for low-frequency applications due to their lower resistivity than Ni-Zn ferrites [18].

Figure 1.1 depicts a variety of Mn-Zn ferrite applications. Changes in cation concentration [19] and sintering conditions [20] alter the magnetic, electrical, and structural characteristics of nano-

Structural and Magnetic Study of Manganese Substituted Zinc Ferrite ($Mn_xZn_{1-x}Fe_2O_4$)
Nanostructures Synthesized via Citric Acid assisted Solgel Autocombustion Method

ferrites, resulting in a wide range of applications. Furthermore, the cation distribution in the Mn-Zn ferrite influences its form, morphology, electrical and magnetic characteristics [21].

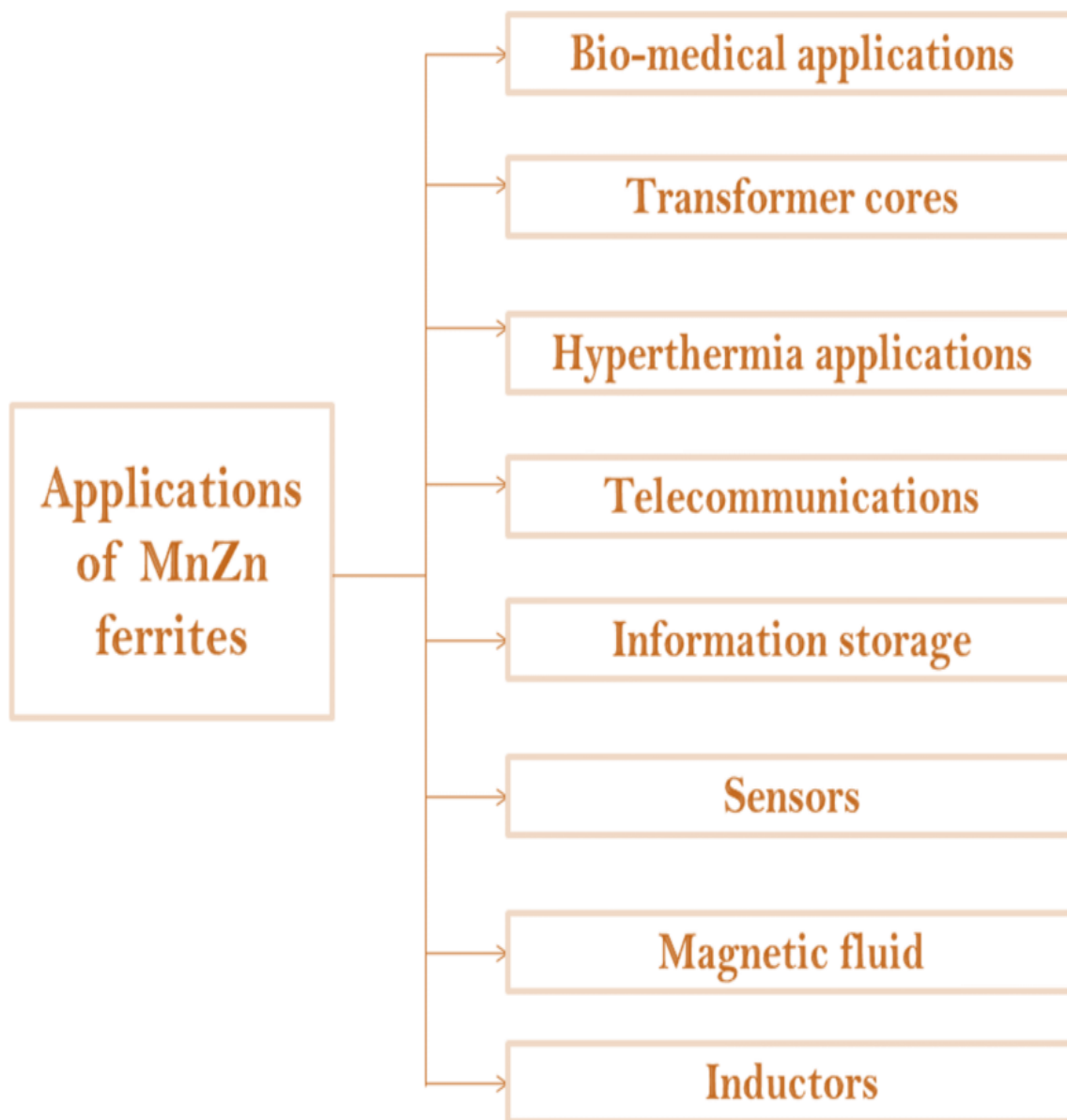


Fig. 1.1: Various applications of Mn-Zn ferrites [22]

The characteristics of Mn-Zn ferrites are determined mainly by the techniques of synthesis [23,24] and the doping concentrations to nano-ferrites [25, 26]. Compared to the other methods, the solgel auto-combustion process is the most cost-effective and ideal for large

production. The sol-gel approach produces the finest crystallites with the greatest morphological control among all synthesis procedures.

Given the relevance of Mn-Zn ferrites in various applications, the current study examines the effect of Mn²⁺ cation substitution on Zn²⁺ in nanoparticles Mn_xZn_{1-x}Fe₂O₄ (X = 0.00, 0.15, 0.30, 0.45) ferrites produced through the sol-gel auto-combustion process. The influence of manganese contents on the microstructure and magnetic characteristics of Mn_xZn_{1-x}Fe₂O₄ ferrites (with X ranging from 0.3 to 0.45) were studied.

1.2. Experimentation

1.2.1. Precursor Materials

Zinc Nitrate [Zn(NO₃)₂.6H₂O], Ferric Nitrate [Fe(NO₃)₃.9H₂O], and Manganese Nitrate [Mn(NO₃)₂.4H₂O] are the essential precursor chemicals for the manufacturing of Mn-Zn ferrite nanoparticles. These compounds were bought with grade purity (purity 99.9%) from Sigma-Aldrich. Citric acid with a purity of 99% was also purchased from Thermo Scientific Company. To keep the pH stable, an ammonia solution was utilized. As a solvent, double-distilled water was utilized.

1.2.2. Synthesis procedure

Citric acid aided sol-gel auto-combustion technology is used to synthesize manganese substituted zinc ferrite nanostructures. A stoichiometric quantity of Zn(NO₃)₂.6H₂O, Mn(NO₃)₂.4H₂O, Fe(NO₃)₃.9H₂O, and C₆H₈O₇ were combined homogeneously in 100 ml double-distilled water to make pure Mn-Zn-ferrite nanoparticles. At 90°C, the combined solution is put on a magnetic stirrer. The pH of the solution is kept at 7 by adding ammonium hydroxide drop by drop. During evaporation, a viscous, sticky gel forms; after drying, it self-ignites and transforms into as-burnt ferrite powder. The as-burnt powder is eventually turned into a fine powder after being completely ground. Finally, the as-prepared fine powder is calcined at 1000°C for 3 hours to get highly crystalline ferrite powder suitable for different characterizations. Figure 1.2 depicts the representation diagram of the auto-combustion sol-gel technique.

Structural and Magnetic Study of Manganese Substituted Zinc Ferrite ($Mn_xZn_{1-x}Fe_2O_4$)
Nanostructures Synthesized via Citric Acid assisted Solgel Autocombustion Method

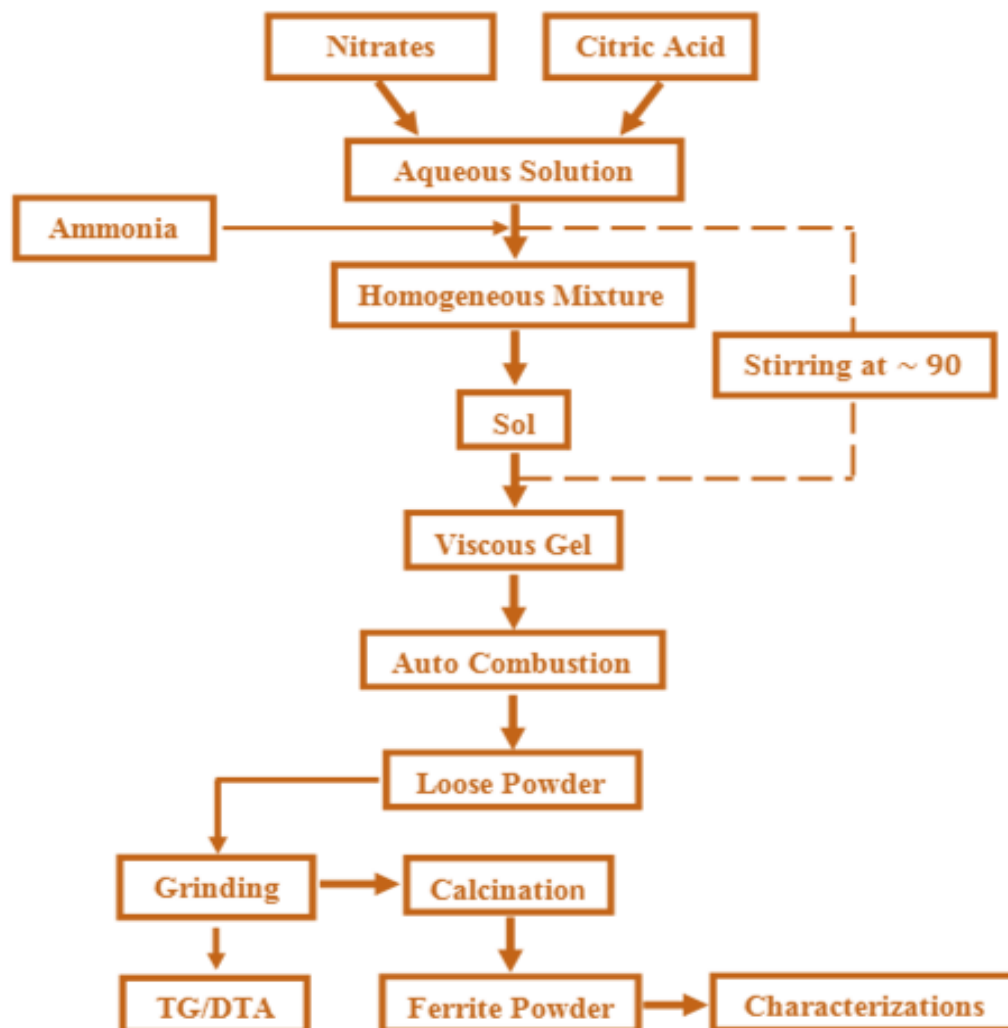


Figure 1.2: Schematic diagram of auto-combustion sol-gel method

1.3. Characterization Techniques

The powder X-ray diffractograms recorded by model PANalytical X'pert PRO with CuK(=1.5406) radiation were used to study the crystalline phases of the manufactured sample. Scanning Electron Microscopy (SEM) was used to assess the morphology of prepared materials (Model- JEOL JSM-6360). A Vibrating Sample Magnetometer (Model-Lakeshore 7404) was utilized to conduct magnetic investigations at room temperature with a 20,000 Gauss applied magnetic field.

1.4. Results and Discussion

1.4.1. Structural Analysis

X-Ray Diffraction is an essential method for studying crystal structure as well as other physical aspects of nanoparticles such as crystallite size, material density, and lattice constant. An X-ray diffraction technique with 2θ varying from 15° to 80° was used to characterize the particles of the $\text{Mn}_x\text{Zn}_{1-x}\text{Fe}_2\text{O}_4$ ($X = 0.00, 0.15, 0.30, 0.45$) series. Figure 1.3 depicts the XRD patterns of all Mn–Zn ferrite nanoparticles produced using the auto-combustion approach. The intense peaks (220), (311), (222), (400), (422), (511), (440), (620), and (533) in the XRD pattern confirmed the formation of Mn–Zn nanoferrites as these peaks match with the Joint Committee on Powder Diffraction Standards (JCPDS) card number #74-2401 and revealed single cubic spinel phase (with $Fd3m$ space group) in all the $\text{Mn}_x\text{Zn}_{1-x}\text{Fe}_2\text{O}_4$ ($X = 0.00, 0.15, 0.30, 0.45$) samples without impurity peaks.

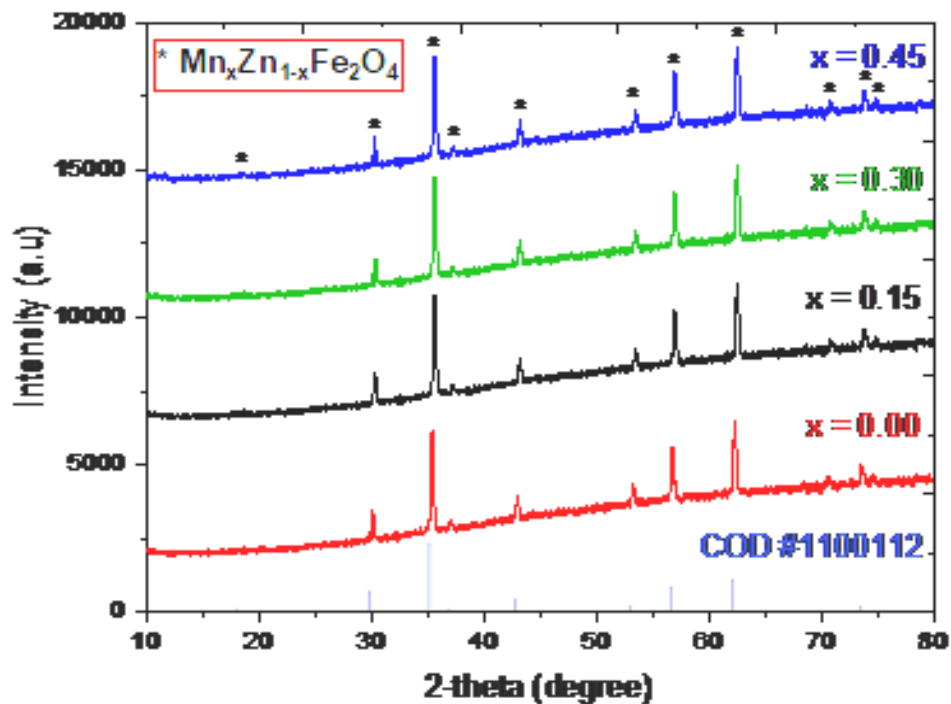


Fig.1.3 XRD pattern of $\text{Mn}_x\text{Zn}_{1-x}\text{Fe}_2\text{O}_4$ ($X = 0.00, 0.15, 0.30, 0.45$) nanoparticles.

The average crystallite size of the nanoferrites, calculated from the most intense peak 311, were found within a range of 28 to 35 nm as determined by Debye - Scherrer's formula as:

Structural and Magnetic Study of Manganese Substituted Zinc Ferrite ($Mn_xZn_{1-x}Fe_2O_4$)
 Nanostructures Synthesized via Citric Acid assisted Solgel Autocombustion Method

$$D_x = \frac{0.9\lambda}{\beta \cos\theta} \text{ nm}$$

Where λ , β , and θ are the X-ray wavelength, full width at half maximum (FWHM) in radians & Bragg's diffraction angle in degrees, respectively [27].

The lattice parameter 'a' values of Ni-Zn ferrite samples were calculated by using Bragg's equation

$$a = \sqrt{d^2(h^2 + k^2 + l^2)} \text{ \AA}$$

Where d is the inter-planer distance and h, k & l are the Miller indices of the XRD diffraction plane.

X-ray density (ρ_x) values were determined by [28].

$$\rho_x = \frac{8M}{Na^3} \text{ g/cm}^3$$

Where '8' represents an 8-formula unit in a unit cell, M is the molecular weight of the samples, N is the Avogadro's number ($6.02252 \times 10^{23} \text{ mol}^{-1}$), and a is the lattice constant.

Lattice constant (a), the crystallite size (D_x), X-ray density (ρ_x) obtained in the present study are listed in Table 1.1.

Table 1.1: Lattice constant (a), the crystallite size (D_x), X-ray density (ρ_x) of $Mn_xZn_{1-x}Fe_2O_4$ (X = 0.00, 0.15, 0.30, 0.45)

| Sample (X) $Mn_xZn_{1-x}Fe_2O_4$ | Crystalline Size(D_x) (nm) | Lattice Constant (a) (\AA) | Density(ρ_x) (gcm^{-3}) |
|-------------------------------------|-----------------------------------|----------------------------------|---------------------------------------|
| X = 0.00 | 28.5 | 8.442 | 5.32 |
| X = 0.15 | 30.3 | 8.458 | 5.25 |

| | | | |
|----------|------|-------|------|
| X = 0.30 | 33.6 | 8.471 | 5.20 |
| X = 0.45 | 35.1 | 8.480 | 5.14 |

Figure 1.4-a depicts the change in lattice parameter 'a' for $Mn_xZn_{1-x}Fe_2O_4$ powders ($X = 0.00, 0.15, 0.30, 0.45$) with Mn^{2+} ion replacement X changing from 0.00 to 0.45. The findings show that many Mn^{2+} and Zn^{2+} ions occupy octahedral positions. As a result, the lattice parameter and unit cell size increase because Mn^{2+} ions substitute for Zn^{2+} ions on the tetrahedral sites in $Mn_xZn_{1-x}Fe_2O_4$. A change in the Mn^{2+} ion ratio resulted in a measurable change in the lattice parameter. The movement of peak locations towards higher diffraction angles is directly connected to lattice parameters. The lattice parameter increased from 8.43 ($X = 0.00$) to 8.48 ($X = 0.45$), while the X-ray density (ρ_x) declined from 5.3 to 5.1 g/cm³. These findings were ascribed to the gradual dissolution of Mn^{2+} ions into the spinel structure, as well as the magnetic performance of the Mn-Zn ferrite, which resulted from a significant number of Mn^{2+} ions with large ionic radii (0.82) replacing the Zn^{2+} ion with smaller ionic radii (0.74) [29, 30, 31].

As demonstrated in figure 1.4-b, the crystallite size increased by increasing the Mn^{2+} ion molar ratio. As a result, when the Mn^{2+} ion ratio increased from 0.00 to 0.45, it increased from 28 to 35 nm. Figure 1.6 also depicts the fluctuation of X-ray density with lattice constant 'a'.

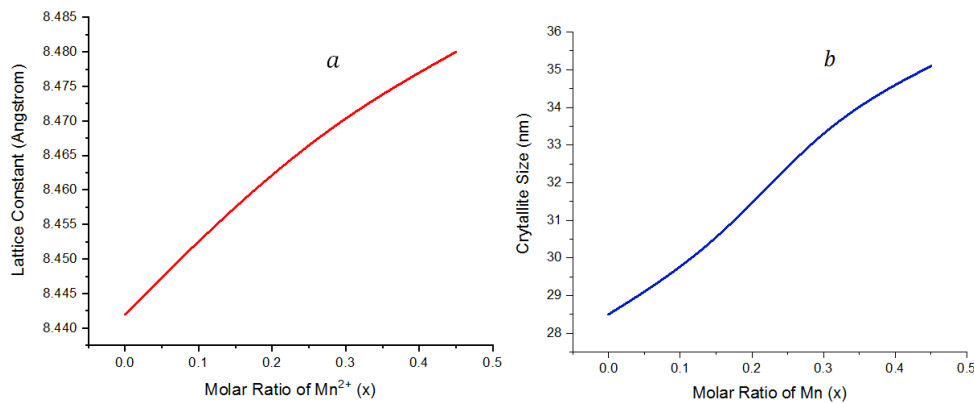


Fig.1.4: (a) Effect of Mn concentration on the lattice parameters of $Mn_xZn_{1-x}Fe_2O_4$ powders with X varying from 0.00 to 0.45. (b) Effect of Mn^{2+} ion substitution on the crystallite size of $Mn_xZn_{1-x}Fe_{2-x}O_4$ ($X = 0.00, 0.15, 0.30, 0.45$) powders

Structural and Magnetic Study of Manganese Substituted Zinc Ferrite ($\text{Mn}_x\text{Zn}_{1-x}\text{Fe}_2\text{O}_4$)
Nanostructures Synthesized via Citric Acid assisted Solgel Autocombustion Method

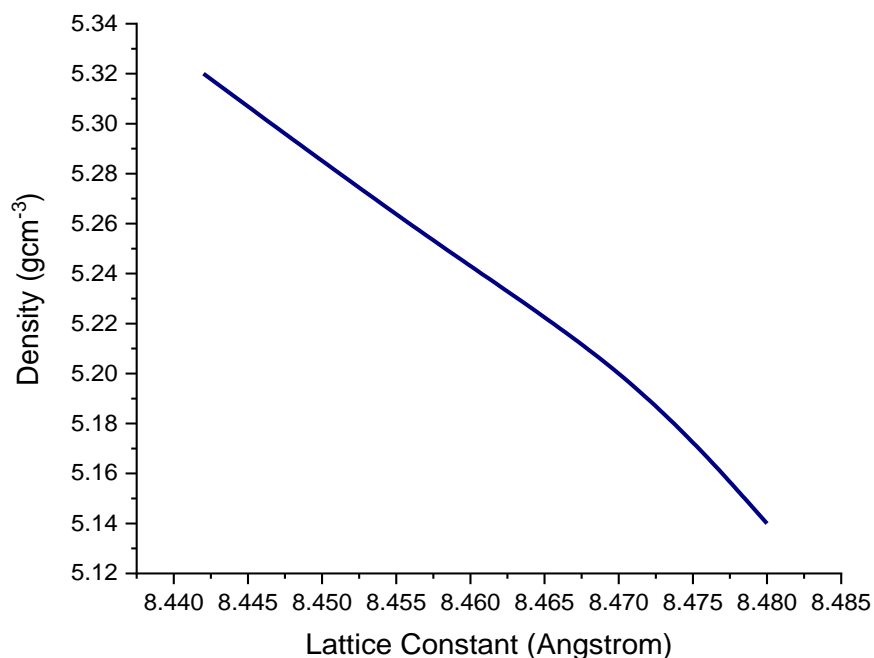


Fig.1.5: Plot between X-Ray density (ρ_x) and Lattice Constant (a)

1.4.2. Morphological Analysis

Scanning Electron Microscopy (SEM) micrographs of $\text{Mn}_x\text{Zn}_{1-x}\text{Fe}_2\text{O}_4$ ($X = 0.00, 0.15, 0.30, 0.45$) nanoferrites sintered at 1000°C for all compositions are shown in Fig. 1.6. (a-d). According to SEM pictures, manganese molar ratios have a noteworthy influence on the morphology of $\text{Mn}_x\text{Zn}_{1-x}\text{Fe}_2\text{O}_4$ ($X = 0.00, 0.15, 0.30, 0.45$). The production of almost spherical nanoferrites particles may be seen in the micrographs. It can also be seen that the particle size increases when the concentration of Mn^{2+} increases from $X = 0.00$ to $X = 0.45$. As a result of the increased Mn^{2+} doping, the majority of nanoparticles have an agglomerated shape and a homogenous distribution. Particles have a roughly spherical form and a narrow size distribution that is almost homogenous. The average particle sizes of the nanoparticles, as estimated by the “image j software”, are in the range of 19 to 41 nm, which are in agreement with XRD results.

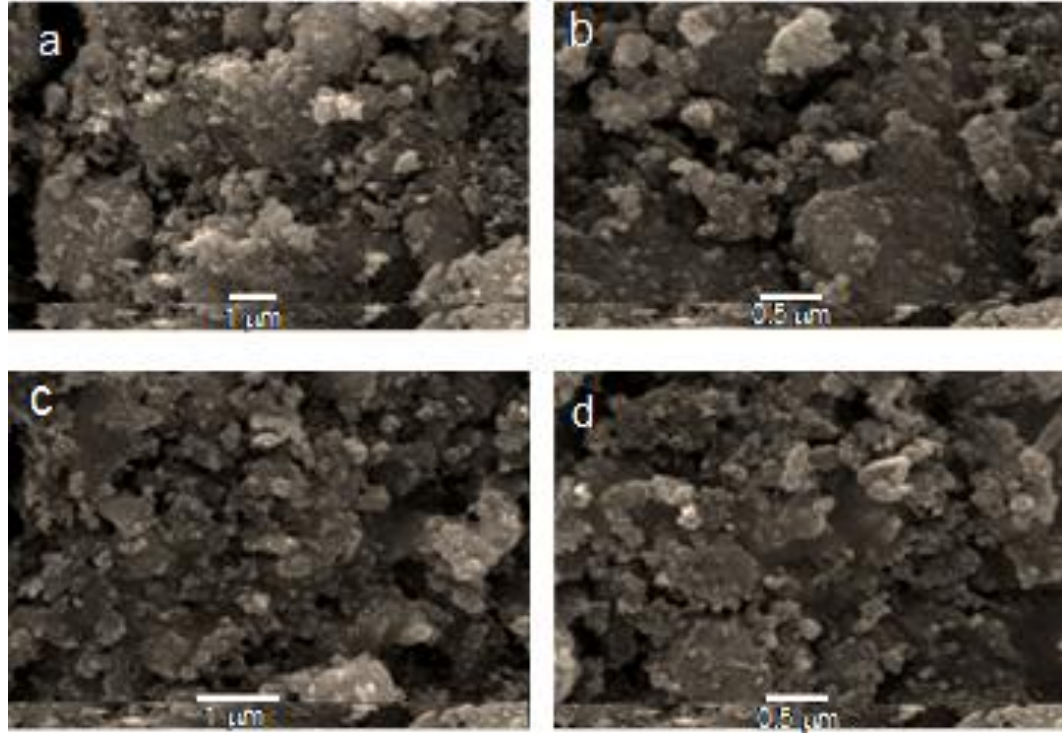


Fig. 1.6 SEM micrographs of a) $\text{Mn}_{0.00}\text{Zn}_1\text{Fe}_2\text{O}_4$, b) $\text{Mn}_{0.15}\text{Zn}_{0.85}\text{Fe}_2\text{O}_4$ c) $\text{Mn}_{0.30}\text{Zn}_{0.70}\text{Fe}_2\text{O}_4$
d) $\text{Mn}_{0.45}\text{Zn}_{0.55}\text{Fe}_2\text{O}_4$

1.4.3. Magnetic Studies

Vibrating Sample Magnetometry (VSM) is a technique for measuring the magnetic characteristics of nanoparticles, namely saturation magnetization (M_s), coercivity (H_c), and residual magnetization (M_r). Mn-Zn ferrites have a high saturation magnetization (M_s), which is why they are often employed in power applications. The magnetization that remains in the absence of an induced magnetic field is known as remanent magnetization (M_r). Mn-Zn ferrites have a poor value for (M_r). Coercivity (H_c) is a ferromagnetic material's capacity to endure an external magnetic field without demagnetization. The M-H curve of $\text{Mn}_x\text{Zn}_{1-x}\text{Fe}_2\text{O}_4$ ($X = 0.00, 0.15, 0.30, 0.45$) nanoferrites at room temperature is shown in Figure 1.7.

Structural and Magnetic Study of Manganese Substituted Zinc Ferrite ($Mn_xZn_{1-x}Fe_2O_4$) Nanostructures Synthesized via Citric Acid assisted Solgel Autocombustion Method

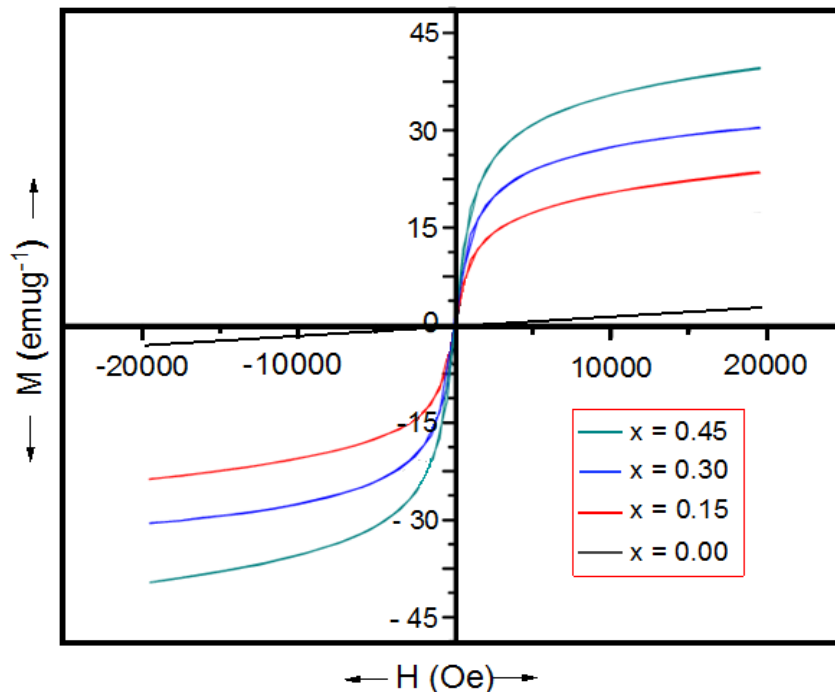


Fig.1.7: M-H plot of $Mn_xZn_{1-x}Fe_2O_4$ ($x = 0.00$ to 0.45) nanoferrites at room temperature

Table 1.2 depicts the essential magnetic characteristics, Saturation Magnetization (M_s), Remanence Magnetization (M_r), and Coercive Field (H_c) of several samples obtained from the plot. The graphs reveal that remanence and coercivity have extremely low values. When demonstrated in Fig.1.7, the coercivity (H_c), saturation magnetization (M_s), and retentivity (M_r), increased as Mn^{2+} concentration rose. Except for $X = 0.00$, the loops for all samples demonstrate superparamagnetic behaviour with very low coercivity values.

Table 1.2: Magnetic parameters like Saturation Magnetization (M_s), Remanence Magnetization (M_r), Coercive Field (H_c) and Magnetic Moment (μ_B) of $Mn_xZn_{1-x}Fe_2O_4$ ($X = 0.00, 0.15, 0.30, 0.45$) ferrite nanoparticles.

| $Mn_xZn_{1-x}Fe_2O_4$ | Saturation Magnetization (emu/g) | Coercivity (Oe) | Magnetic Moment (μ_B) |
|-----------------------|----------------------------------|-----------------|-----------------------------|
| $X = 0.00$ | 4 | 0 | 0.1 |

| | | | |
|----------|----|----|-----|
| X = 0.15 | 23 | 15 | 1.0 |
| X = 0.30 | 28 | 23 | 1.2 |
| X = 0.45 | 39 | 30 | 1.7 |

Clearly, increasing the Mn^{2+} molar ratio from 0.00 to 0.45, the (M_s) value increased from 4 emu/g to 39 emu/g, and the coercivity value also increased from 0 to 30 Oe, when the particle size improved from 28 to 35 nm, as listed in Table 1.2. The variation of Magnetization with concentration and crystalline size; and magnetic moment with Mn^{2+} concentration is shown in figure 1.8 (b-d).

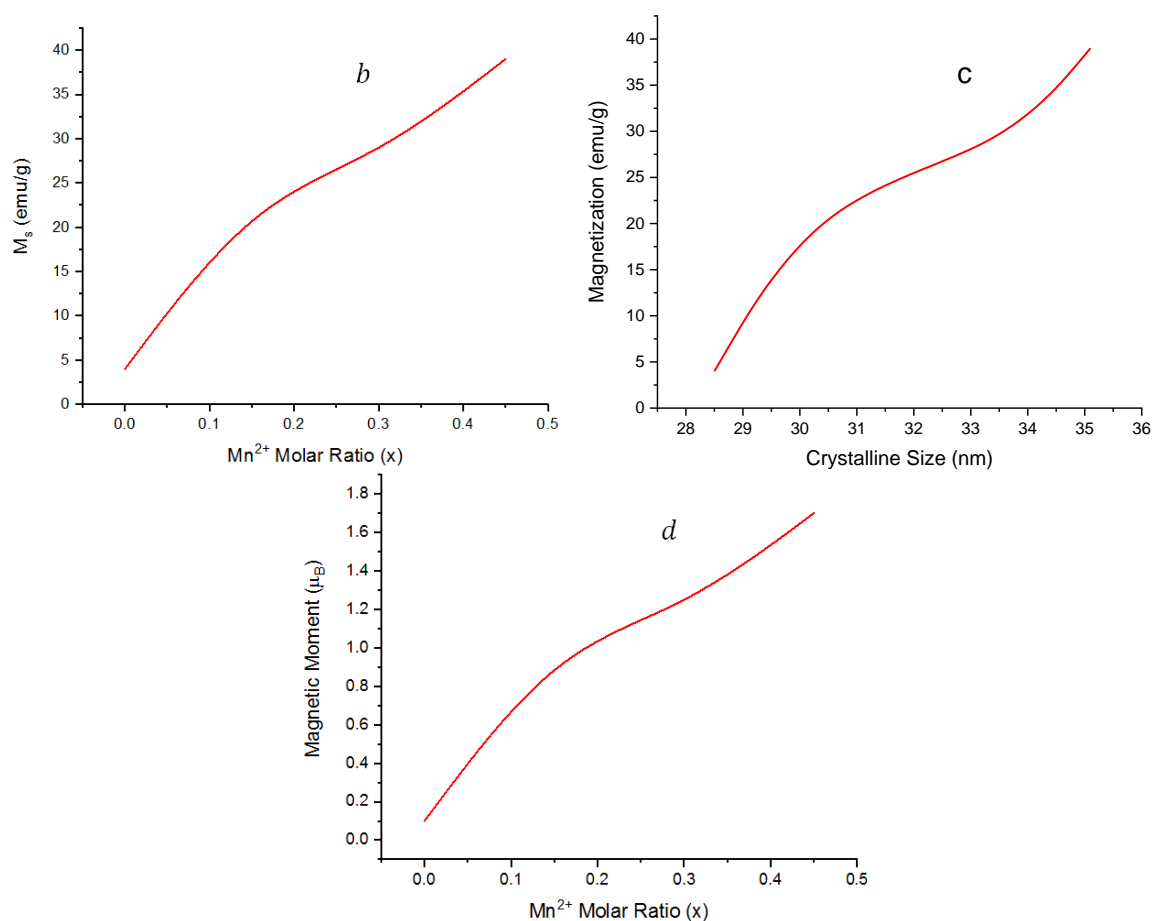


Fig.1.8: Variation of Magnetization with a) Mn^{2+} concentration b) Crystalline size; and magnetic moment with Mn^{2+} concentration.

Structural and Magnetic Study of Manganese Substituted Zinc Ferrite ($Mn_xZn_{1-x}Fe_2O_4$)
Nanostructures Synthesized via Citric Acid assisted Solgel Autocombustion Method

Changes in magnetic characteristics of nanoparticles such as coercivity (H_c), saturation magnetization (M_s), and retentivity (M_r) are caused by the surface effect, cationic stoichiometry, and occupancy at particular sites [32, 33].

Manganese ions preferentially occupy the octahedral B site when manganese ion concentration increases, resulting in an equivalent amount of trivalent iron ions occupying the tetrahedral A-site. The magnetic moment $\mu_B (\chi)$ in the Néel model may be described using the following equation: [34]

$$\mu_B (\chi) = M_B (\chi) - M_A (\chi)$$

In this formula, $M_B (\chi)$ and $M_A (\chi)$ indicate the magnetic moments of the tetrahedral structure position (A) and octahedral structure position (B) in the Mn-Zn ferrite, respectively. The magnetic moment $\mu_B (\chi)$ is deeply linked to the structural position, metal cation distribution, and the spin effect. Spinel ferrite's magnetic order is caused by the super-exchange interaction process of metal ions at the A and B sites.

As the concentration of Mn^{2+} increases, so does the magnetic moment μ_B . This is because Mn^{2+} preferentially occupies position B of the octahedron structure, forcing the equal quantity of Fe^{3+} in the reaction system to enter position A of the tetrahedron structure. This causes a progressive rise in the super-exchange force between A–B sites, net magnetic moment, and saturation magnetization. μ_B is the experimental value of the ferrite's magnetic moment, which may be derived using the following formula: [35]

$$\mu_B = \frac{M_w \times M_s}{5585}$$

μ_B = Experimental magnetic moment; M_w = Molecular weight; M_s = Saturation magnetization.

Table 1 shows the computation results for μ_B . Magnetic moment μ_B computed values indicate an increasing trend from 0.1 to 1.7 with an increasing molar ratio of Mn^{2+} ions in Mn-Zn spinel ferrites. The table shows that the magnetic moment and saturation magnetization are closely connected, and that μ_B is proportional to M_s .

It has previously been stated that such superparamagnetic materials with low coercivity might be helpful in Hyperthermia, MRI Magnetic Resonance Imaging (MRI), and Drug Delivery applications.

1.5. Conclusion

For Mn-Zn ferrite nanoparticles, the following conclusions are drawn from the XRD, SEM, and VSM observations:

- Nanocrystalline $Mn_xZn_{1-x}Fe_2O_4$ ($X = 0.00, 0.15, 0.30, 0.45$) ferrite powders have been prepared using a simple citric acid aided sol-gel auto-combustion technique.
- XRD measurements verified the synthesis of a cubic spinel structure with relatively tiny crystallite sizes ranging from 25 nm to 35 nm, and the lattice constant (a) rose somewhat as the Mn^{2+} ratio increased.
- SEM micrographs show that $Mn_xZn_{1-x}Fe_2O_4$ ($X = 0.00, 0.15, 0.30, 0.45$) ferrite powder has a homogenous compact sphere-like structure. The average particle sizes of the nanoparticles, as estimated by the “image j software”, are in the range of 19 to 41 nm which matches with X-Ray diffraction results.
- The magnetic moment, saturation magnetization, and coercivity improved from 0.1 to 1.7, 4 to 39 emu/g, and 1 to 30 Oe, respectively, when the Mn^{2+} molar ratio grew from 0.00 to 0.45.
- The graphs for all samples, excluding $X = 0.00$, show superparamagnetic behaviour with very low coercivity values.
- As a result of their tunable and enhanced superparamagnetic characteristics, the investigated spinel Mn-Zn mixed ferrite system may be helpful in a variety of applications such as hyperthermia, drug delivery, and Magnetic Resonance Imaging (MRI).

1.6. References

- [1] Tatarchuk, T. R., Bououdina, M., Paliychuk, N. D., Yaremiy, I. P., & Moklyak, V. V. (2017). Structural characterization and antistructure modeling of cobalt-substituted zinc

Structural and Magnetic Study of Manganese Substituted Zinc Ferrite ($Mn_xZn_{1-x}Fe_2O_4$)
Nanostructures Synthesized via Citric Acid assisted Solgel Autocombustion Method

- ferrites. *Journal of Alloys and Compounds*, 694, 777-791.
<https://doi.org/10.1016/j.jallcom.2016.10.067>.
- [2] Song, Q., & Zhang, Z. J. (2012). Controlled synthesis and magnetic properties of bimagnetic spinel ferrite $CoFe_2O_4$ and $MnFe_2O_4$ nanocrystals with core-shell architecture. *Journal of the American Chemical Society*, 134(24), 10182-10190.
<https://doi.org/10.1021/ja302856z>.
- [3] Namai, A., Yoshikiyo, M., Yamada, K., Sakurai, S., Goto, T., Yoshida, T., ... & Ohkoshi, S. I. (2012). Hard magnetic ferrite with a gigantic coercivity and high frequency millimetre wave rotation. *Nature communications*, 3(1), 1-6.
- [4] Mansour, S. F., Hemeda, O. M., Abdo, M. A., & Nada, W. A. (2018). Improvement on the magnetic and dielectric behavior of hard/soft ferrite nanocomposites. *Journal of Molecular Structure*, 1152, 207-214.
- [5] Modaresi, N., Afzalzadeh, R., Aslibeiki, B., Kameli, P., Varzaneh, A. G., Orue, I., & Chernenko, V. A. (2019). Magnetic properties of $Zn_xFe_{3-x}O_4$ nanoparticles: A competition between the effects of size and Zn doping level. *Journal of Magnetism and Magnetic Materials*, 482, 206-218.
- [6] Torkian, S., Ghasemi, A., & Razavi, R. S. (2016). Magnetic properties of hard-soft $SrFe_{10}Al_2O_{19}/Co_{0.8}Ni_{0.2}Fe_2O_4$ ferrite synthesized by one-pot sol-gel auto-combustion. *Journal of Magnetism and Magnetic Materials*, 416, 408-416.
- [7] He, S., Zhang, H., Liu, Y., Sun, F., Yu, X., Li, X., ... & Zeng, H. (2018). Maximizing specific loss power for magnetic hyperthermia by hard-soft mixed ferrites. *Small*, 14(29), 1800135.
- [8] Zhao, H., Ragusa, C., Appino, C., de la Barrière, O., Wang, Y., & Fiorillo, F. (2018). Energy losses in soft magnetic materials under symmetric and asymmetric induction waveforms. *IEEE Transactions on Power Electronics*, 34(3), 2655-2665.

- [9] Füzér, J., Strečková, M., Dobák, S., Ďáková, E., Kollár, P., Fáberová, M., ... & Vojtko, M. (2018). Innovative ferrite nanofibres reinforced soft magnetic composite with enhanced electrical resistivity. *Journal of Alloys and Compounds*, 753, 219-227.
- [10] Töpfer, J., Mürbe, J., Angermann, A., Kracunovska, S., Barth, S., & Bechtold, F. (2006). Soft ferrite materials for multilayer inductors. *International journal of applied ceramic technology*, 3(6), 455-462. <https://doi.org/10.1111/j.1744-7402.2006.02110.x>
- [11] Kogias, G., Holz, D., & Zaspalis, V. (2014). New MnZn ferrites with high saturation flux density. *Journal of the Japan Society of Powder and Powder Metallurgy*, 61(S1), S201-S203. <https://doi.org/10.2497/jjspm.61.s201>.
- [12] Venturini, J., Tonelli, A. M., Wermuth, T. B., Zampiva, R. Y. S., Arcaro, S., Viegas, A. D. C., & Bergmann, C. P. (2019). Excess of cations in the sol-gel synthesis of cobalt ferrite (CoFe₂O₄): A pathway to switching the inversion degree of spinels. *Journal of Magnetism and Magnetic Materials*, 482, 1-8. <https://doi.org/10.1016/j.jmmm.2019.03.057>.
- [13] Javed, H., Iqbal, F., Agboola, P. O., Khan, M. A., Warsi, M. F., & Shakir, I. (2019). Structural, electrical and magnetic parameters evaluation of nanocrystalline rare earth Nd³⁺-substituted nickel-zinc spinel ferrite particles. *Ceramics International*, 45(8), 11125-11130. <https://doi.org/10.1016/j.ceramint.2019.02.176>.
- [14] Sánchez, J., Cortés-Hernández, D. A., & Rodríguez-Reyes, M. (2019). Synthesis of TEG-coated cobalt-gallium ferrites: characterization and evaluation of their magnetic properties for biomedical devices. *Journal of Alloys and Compounds*, 781, 1040-1047. <https://doi.org/10.1016/j.jallcom.2018.12.052>.
- [15] Ali, M. A., Khan, M. N. I., Hossain, M. M., Chowdhury, F. U. Z., Hossain, M. N., Rashid, R., ... & Uddin, M. M. (2020). Mechanical behavior, enhanced dc resistivity, energy band gap and high temperature magnetic properties of Y-substituted Mg–Zn ferrites. *Materials Research Express*, 7(3), 036101. <https://doi.org/10.1088/2053-1591/ab7791>.
- [16] Choudhari, S. S., Shelke, S. B., Batoo, K. M., Adil, S. F., Kadam, A. B., Imran, A., ... & Kadam, R. H. (2021). Mn_{0.7}Zn_{0.3}Fe₂O₄+ BaTiO₃ composites: structural, morphological,

Structural and Magnetic Study of Manganese Substituted Zinc Ferrite ($Mn_xZn_{1-x}Fe_2O_4$)
Nanostructures Synthesized via Citric Acid assisted Solgel Autocombustion Method

- magnetic, M–E effect and dielectric properties. *Journal of Materials Science: Materials in Electronics*, 32(8), 10308-10319. <https://doi.org/10.1007/s10854-021-05686-z>.
- [17] Li, M., Fang, H., Li, H., Zhao, Y., Li, T., Pang, H., ... & Liu, X. (2017). Synthesis and characterization of MnZn ferrite nanoparticles with improved saturation magnetization. *Journal of Superconductivity and Novel Magnetism*, 30(8), 2275-2281. <https://doi.org/10.1007/s10948-017-4013-9>.
- [18] Fu, C. M., Syue, M. R., Wei, F. J., Cheng, C. W., & Chou, C. S. (2010). Synthesis of nanocrystalline Ni–Zn ferrites by combustion method with no postannealing route. *Journal of Applied Physics*, 107(9), 09A519. <https://doi.org/10.1063/1.3337689>
- [19] Bamzai, K. K., Kour, G., Kaur, B., & Kulkarni, S. D. (2013). Effect of cation distribution on structural and magnetic properties of Dy substituted magnesium ferrite. *Journal of magnetism and magnetic materials*, 327, 159-166. <https://doi.org/10.1016/j.jmmm.2012.09.013>.
- [20] Beatrice, C., Dobák, S., Tsakaloudi, V., Ragusa, C., Fiorillo, F., Martino, L., & Zaspalis, V. (2018). Magnetic loss, permeability, and anisotropy compensation in CoO-doped Mn-Zn ferrites. *AIP Advances*, 8(4), 047803. <https://doi.org/10.1063/1.4993718>.
- [21] Thota, S., Kashyap, S. C., Sharma, S. K., & Reddy, V. R. (2016). Cation distribution in Ni-substituted $Mn_{0.5}Zn_{0.5}Fe_2O_4$ nanoparticles: a Raman, Mössbauer, X-ray diffraction and electron spectroscopy study. *Materials Science and Engineering: B*, 206, 69-78. <https://doi.org/10.1016/j.mseb.2016.01.002>
- [22] A, Thakur, P., Taneja, S., Sindhu, D., Lüders, U., Sharma, A., Ravelo, B., & Thakur, A. (2020). Manganese zinc ferrites: a short review on synthesis and characterization. *Journal of Superconductivity and Novel Magnetism*, 33(6), 1569-1584.

- [23] Szczygieł, I., & Winiarska, K. (2014). Synthesis and characterization of manganese–zinc ferrite obtained by thermal decomposition from organic precursors. *Journal of Thermal Analysis and Calorimetry*, 115(1), 471-477. <https://doi.org/10.1007/s10973-013-3281-2>.
- [24] Meng, Y. Y., Liu, Z. W., Dai, H. C., Yu, H. Y., Zeng, D. C., Shukla, S., & Ramanujan, R. V. (2012). Structure and magnetic properties of Mn (Zn) Fe_{2-x}RE_xO₄ ferrite nano-powders synthesized by co-precipitation and refluxing method. *Powder Technology*, 229, 270-275. <https://doi.org/10.1016/j.powtec.2012.06.050>.
- [25] Thakur, A., Thakur, P., & Hsu, J. H. (2014). Structural, magnetic and electromagnetic characterization of In³⁺ substituted Mn-Zn nanoferrites. *Zeitschrift für Physikalische Chemie*, 228(6-7), 663-672. <https://doi.org/10.1515/zpch-2014-0477>.
- [26] Thakur, A., Mathur, P., & Singh, M. (2007). Controlling the properties of manganese-zinc ferrites by substituting In³⁺ and Al³⁺ ions. *Zeitschrift für Physikalische Chemie*, 221(6), 837-845. <https://doi.org/10.1524/zpch.2007.221.6.837>.
- [27] Cullity, B. D. (1978). *Answers to problems: elements of X-ray diffraction*. Addison-Wesley Publishing Company.
- [28] Smith, J., & Wijn, H. P. J. (1959). *Ferrites Wiley. Inc.. New York*, 229.
- [29] Hessian, M. M., Rashad, M. M., & El-Barawy, K. (2008). Controlling the composition and magnetic properties of strontium hexaferrite synthesized by co-precipitation method. *Journal of magnetism and magnetic materials*, 320(3-4), 336-343.
- [30] Henderson, C. M. B., Charnock, J. M., & Plant, D. A. (2007). Cation occupancies in Mg, Co, Ni, Zn, Al ferrite spinels: a multi-element EXAFS study. *Journal of Physics: Condensed Matter*, 19(7), 076214.
- [31] Rath, C., Sahu, K. K., Anand, S., Date, S. K., Mishra, N. C., & Das, R. P. (1999). Preparation and characterization of nanosize Mn–Zn ferrite. *Journal of magnetism and magnetic materials*, 202(1), 77-84.

Structural and Magnetic Study of Manganese Substituted Zinc Ferrite ($\text{Mn}_x\text{Zn}_{1-x}\text{Fe}_2\text{O}_4$)
Nanostructures Synthesized via Citric Acid assisted Solgel Autocombustion Method

- [32] Arulmurugan, R., Vaidyanathan, G., Sendhilnathan, S., & Jeyadevan, B. (2006). Mn–Zn ferrite nanoparticles for ferrofluid preparation: study on thermal–magnetic properties. *Journal of magnetism and magnetic materials*, 298(2), 83-94.
- [33] Hiroki, T., Taira, S., Katayanagi, H., Moro, Y., Shigeoka, D., Kimura, S., ... & Ichiyanagi, Y. (2010). Functional magnetic nanoparticles for use in a drug delivery system. In *Journal of Physics: Conference Series* (Vol. 200, No. 12, p. 122003). IOP Publishing.
- [34] Tsakaloudi, V., Holz, D., & Zaspalis, V. (2013). The effect of externally applied uniaxial compressive stress on the magnetic properties of power MnZn-ferrites. *Journal of Materials Science*, 48(10), 3825-3833. doi:10.1007/s10853-013-7183-2
- [35] Li, D. G., Chen, C., Rao, W., Lu, W. H., & Xiong, Y. H. (2014). Preparation and microwave absorption properties of polyaniline/ $\text{Mn}_{0.8}\text{Zn}_{0.2}\text{Fe}_2\text{O}_4$ nanocomposite in 2–18 GHz. *Journal of Materials Science: Materials in Electronics*, 25(1), 76-81.